Periodicity and Chaos Amidst Twisting and Folding in Two-Dimensional Maps

Garst, S.; Sterk, A.E.

Published in:
International Journal of Bifurcation and Chaos

DOI:
10.1142/S0218127418300124

Publication date:
2018

Periodicity and chaos amidst twisting and folding in 2-dimensional maps

S. Garst A.E. Sterk

May 7, 2018

Abstract

We study the dynamics of three planar, non-invertible maps which rotate and fold the plane. Two maps are inspired by real-world applications whereas the third map is constructed to serve as a toy model for the other two maps. The dynamics of the three maps are remarkably similar. A stable fixed point bifurcates through a Hopf–Neĭmark–Sacker which leads to a countably infinite set of resonance tongues in the parameter plane of the map. Within a resonance tongue a periodic point can bifurcate through a period doubling cascade. At the end of the cascade we detect Hénon-like attractors which are conjectured to be the closure of the unstable manifold of a saddle periodic point. These attractors have a folded structure which can be explained by means of the concept of critical lines. We also detect snap-back repellers which can either coexist with Hénon-like attractors or which can be formed when the saddle-point of a Hénon-like attractor becomes a source.

Key words: non-invertible maps, bifurcations, Hénon-like attractors, snap-back repellers

Contents

1 Introduction

In this paper we compare the dynamics of three planar, non-invertible maps which all rotate and fold the plane. Two of these maps are related to phenomena in biology and physics, whereas the the third map is *constructed* to serve as a toy model for the other two maps.

1.1 Motivation

An important problem in the mathematical theory of dynamical systems is to determine the geometric structure of chaotic attractors and the bifurcations leading to their formation. Inspiration for the development of the theory often comes from the analytical and numerical study of particular examples, but of course the goal is to understand the dynamics of a large class of systems. Ideally, one would like to classify the behavior of dynamical systems according to some equivalence relation. For example, dynamical systems that are topologically conjugate have identical topological properties, and in particular they share the same number of fixed points and periodic orbits of the same stability types. However, topological conjugacy can only be proved in specific cases. In the vicinity of bifurcations one can use the theory of normal forms. All systems exhibiting a certain type of bifurcation are locally (i.e., around the equilibrium) topologically equivalent to the normal form of the bifurcation Broer and Takens [2010], Guckenheimer and Holmes [1983], Kuznetsov [2004].

A fruitful strategy to understand chaotic dynamics is to construct representative examples that explain the dynamical behavior observed in concrete applications. A well-known example is the *horseshoe map* introduced in Smale [1967, 1998] which has become the hallmark of chaos. The horseshoe map is an Axiom A diffeomorphism that serves as a model for the generic behavior at a transverse homoclinic point at which the stable and unstable manifolds of a periodic point intersect. Another example of this strategy is given by the so-called *geometric Lorenz models* that were constructed to understand the attractor of the Lorenz-63 system [Afraimovich et al., 1977, Guckenheimer and Williams, 1979, Viana, 2000, Williams, 1979]. Such *toy models*, or *models of models*, are of great help to understand complex dynamics.

In many works a similar strategy has been adopted to unravel generic dynamical

features in the vicinity of particular bifurcations. A simplified global model for the return map of a dissipative diffeomorphism near a homoclinic bifurcation was presented in Broer et al. [1998]. This map is a perturbation of the Arnold family of circle maps and its dynamics involves periodicity, quasi-periodicity and chaos, between which there are various transitions bifurcations. This map has a universal character in the setting of 2-dimensional diffeomorphisms and can be compared with examples like the Hénon map and the standard map. Detailed studies of 3-dimensional diffeomorphisms, in particular near a Hopf-saddle-node bifurcation, can be found in [Broer et al., 2008a,b, Vitolo et al., 2010]. These studies were mainly inspired by results obtained for the Poincaré map of the periodically driven Lorenz–84 atmospheric model [Broer et al., 2002]. In the latter map so-called quasi-periodic Hénon-like attractors, which are conjectured to coincide with the unstable manifold of a hyperbolic invariant circle of saddle-type, have been detected [Broer et al., 2005]. The existence of such attractors has been rigorously proved for a map on the solid torus [Broer et al., 2010].

In this paper we are concerned with the study of non-invertible, planar maps. The study of such maps goes back to at least the works [Gumowski and Mira, 1965, 1969, Mira, 1964] in which the role of critical lines in the formation of basin boundaries and their bifurcations was studied. Since the 1990s the interest for 2-dimensional endomorphisms has increased tremendously. For a detailed account, the reader is referred to the textbook of Mira et al. [1996] and the references therein. The aim of this paper is to present a case study of three maps that rotate and fold the plane. Two of these maps are taken from the literature, whereas the third map is constructed to mimic the dynamical features of the other maps. The dynamics of the three maps are remarkable similar, which suggests that their dynamics is generic among planar maps that exhibit rotation and folding.

1.2 Maps of study

We first describe two particular planar maps which rotate and fold the plane. Next, we introduce a model map which is intended to serve as a representative toy model for the other maps.

1.2.1 A predator-prey model

Consider the following planar map

$$\mathscr{P} : \begin{pmatrix} x \\ y \end{pmatrix} \mapsto \begin{pmatrix} ax(1-x-y) \\ bxy \end{pmatrix}. \tag{1}$$

This map is a simplification of the predator-prey model studied in Beddington et al. [1976]; also see Mira et al. [1996] and references therein. In this paper we restrict to the parameter range $1 < a < 5$ and $b > 5/2$.

The map $\mathscr{P}$ is not invertible. Indeed, in the region defined by $ab - 4bx - 4ay > 0$ the map $\mathscr{P}$ has two preimages. Moreover, this map has a fixed point $(\frac{1}{b}, 1 - \frac{1}{a} - \frac{1}{b})$, which has complex eigenvalues for the parameters $b > (a + \sqrt{a})/(2a - 2)$. Hence, the map $\mathscr{P}$ rotates points near this fixed point.

1.2.2 A discretized Lorenz-63 model

Our second example arises from the classical Lorenz-63 model Lorenz [1963, 1989] for Rayleigh-Bénard convection:

$$\frac{dx}{dt} = -\sigma(x - y), \qquad \frac{dy}{dt} = \rho x - y - xz, \qquad \frac{dz}{dt} = -\beta z + xy.$$

Taking the limit $\sigma \to \infty$ and replacing x with y gives a system of two differential equations:

$$\frac{dy}{dt} = (\rho - 1)y - yz, \qquad \frac{dz}{dt} = -\beta z + y^2.$$

In what follows, we will relabel the variables (y, z) as (x, y) again. In this 2-dimensional system we can assume without loss of generality that $\beta = 1$ by a suitable rescaling (but note that this property does not hold for the 3-dimensional system). After discretizing these equations by means of a forward Euler scheme with time step τ we obtain the map

$$\mathscr{L} : \begin{pmatrix} x \\ y \end{pmatrix} \mapsto \begin{pmatrix} (1 + \alpha\tau)x - \tau xy \\ (1 - \tau)y + \tau x^2 \end{pmatrix}, \tag{2}$$

where $\alpha = \rho - 1$. In this paper, we restrict to the parameter range $0 < \alpha < 1$ and $0 < \tau < 4$.

First note, that the map $\mathscr{L}$ is noninvertible. The curve defined by the equation

$$4\tau(y - cb)^3 = 27c^2x^2, \quad c = 1 - \tau, \quad b = (1 + \alpha\tau)/\tau,$$

separates two regions in the plane in which the map has either one or three preimages. In addition, the map has a fixed point $(\pm\sqrt{\alpha}, \alpha)$ of which the eigenvalues are complex for $\alpha > \frac{1}{8}$, see Proposition 2.

1.2.3 The fold-and-twist map

The maps $\mathscr{P}$ and $\mathscr{L}$ rotate points and fold the plane. Our aim is to study the combination of these effects in a map that is as simple as possible. To that end, we first define the map

$$\mathscr{F} : \begin{pmatrix} x \\ y \end{pmatrix} \mapsto \begin{pmatrix} f(x) \\ y \end{pmatrix},$$

where $f : \mathbb{R} \to \mathbb{R}$ is a continuous two-to-one map. Observe that $\mathscr{F}$ maps vertical lines onto vertical lines. In the following we will take

$$f(x) = \tfrac{1}{4}(a-2) - ax^2$$

which is conjugate to the logistic family $g(x) = ax(1-x)$. Indeed, for $\psi(x) = x - \frac{1}{2}$ we have that $f \circ \psi = \psi \circ g$. Hence, we will restrict to the parameter range $a \in [0, 4]$. Next, we consider a rigid rotation around the origin given by

$$\mathscr{R} : \begin{pmatrix} x \\ y \end{pmatrix} \mapsto \begin{pmatrix} x\cos\varphi - y\sin\varphi \\ x\sin\varphi + y\cos\varphi \end{pmatrix}.$$

The "fold-and-twist map" $\mathscr{T}$ is defined as the composition

$$\mathscr{T} = \mathscr{R} \circ \mathscr{F} : \begin{pmatrix} x \\ y \end{pmatrix} \mapsto \begin{pmatrix} f(x)\cos\varphi - y\sin\varphi \\ f(x)\sin\varphi + y\cos\varphi \end{pmatrix}. \tag{3}$$

The angle φ is measured in radians. However, for numerically obtained results values are reported in degrees, which is indicated by means of a subscript: $\varphi_d = 180\varphi/\pi$. It is easy to verify that the maps $\mathscr{T}_{\varphi,a}$ and $\mathscr{T}_{2\pi-\varphi,a}$ are conjugate via $\Psi(x, y) = (x, -y)$. In particular, the bifurcation diagram in the (φ, a)-plane is symmetric with respect to the line $\varphi = \pi$. Therefore, it suffices to study the family $\mathscr{T}_{\varphi,a}$ for $0 \le \varphi \le \pi$.

The dynamical properties of the map $\mathscr{T}$ were explored in Garst and Sterk [2016]. The advantage of the map $\mathscr{T}$ is that the folding and twisting can be controlled separately using the parameters a and φ, and the idea of this paper is that the map $\mathscr{T}$ may serve as a "guide" to study and explain phenomena in the maps $\mathscr{P}$ and $\mathscr{L}$.

Table 1: Color coding for the Lyapunov diagram of Figures 1, 2, and 3. The diagrams suggest that periodic attractors and chaotic attractors with 1 or 2 positive Lyapunov exponents occur for regions in the parameter plane with positive Lebesgue measure.

Color	Lyapunov exponents	Attractor type
cyan	$0 > \lambda_1 > \lambda_2$	periodic point of node type
blue	$0 > \lambda_1 = \lambda_2$	periodic point of focus type
green	$0 = \lambda_1 > \lambda_2$	invariant circle
red	$\lambda_1 > 0 \geq \lambda_2$	chaotic attractor
black	$\lambda_1 \geq \lambda_2 > 0$	chaotic attractor
white		no attractor detected

1.3 Overview of the dynamics

The Lyapunov diagrams in Figures 1–3 show a classification of the dynamical behavior of the maps $\mathscr{P}$, $\mathscr{L}$, and $\mathscr{T}$ in different regions of their parameter planes. See Appendix A for a description of the algorithm used to compute Lyapunov exponents. Note that the three diagrams have a very similar geometric organization. In particular, one can observe a prevalence of periodic dynamics and chaotic dynamics. In all three diagrams one can observe tongue-shaped regions emanating along a curve. This suggests the presence of a Hopf–Neĭmark–Sacker bifurcation. Propositions 1–3 in Section 2.2 confirm that this is indeed the case.

The Lyapunov diagrams also suggest that chaotic attractors with one or two positive Lyapunov exponents occur for regions in the parameter plane with positive Lebesgue measure, and the question is how these attractors are formed and what their geometric structure is. Numerical evidence suggest that strange attractors having one positive Lyapunov exponent are of Hénon-like type, i.e., they are formed by the closure of the unstable manifold of a periodic point of saddle type. However, unlike in diffeomorphisms, these attractors have a folded structure in our maps.

2 Twisting and (quasi-)periodic dynamics

In this section we discuss periodic and quasi-periodic dynamics of the maps $\mathscr{P}$, $\mathscr{L}$, and $\mathscr{T}$. The Lyapunov diagrams already indicate that these type of dynamics occur in large

regions of the parameter plane.

2.1 Preliminaries

We first present some elementary observations that will make the proofs in the following section shorter.

2.1.1 Stability of periodic points

The stability of a period-p point of any differentiable map $\mathscr{F} : \mathbb{R}^2 \to \mathbb{R}^2$ can be determined from the so-called stability triangle [Barreto et al., 1997]. Let T and D denote respectively the trace and the determinant of the Jacobian matrix of $\mathscr{F}^p$ evaluated at the period-p point. The eigenvalues of this matrix are given by

$$\lambda_\pm = \frac{T \pm \sqrt{T^2 - 4D}}{2}.$$

The periodic point is stable when $|\lambda_\pm| < 1$, which is the case if and only if

$$-1 < D < 1 \quad \text{and} \quad -1 - D < T < 1 + D. \tag{4}$$

These inequalities determine a triangular region in the (T, D)-plane, see Figure 4. The eigenvalues are real (resp. complex) for $D \leq T^2/4$ (resp. $D > T^2/4$). The periodic point loses stability by crossing the boundaries of the stability triangle in the following ways:

- Crossing the line $D = 1$ implies that the complex pair $\lambda_\pm$ crosses the unit circle;
- Crossing the line $T = 1 + D$ implies that λ_+ passes through 1;
- Crossing the line $T = -1 - D$ implies that λ_- passes through -1.

2.1.2 The normal form of the Hopf-Neĭmark-Sacker bifurcation

Assume that a differentiable map $\mathscr{F} : \mathbb{R}^2 \to \mathbb{R}^2$ has a fixed point x_0 at which the Jacobian matrix J has two complex conjugate eigenvalues $e^{\pm i\theta}$ on the unit circle. This indicates that the fixed point x_0 bifurcates through a Hopf-Neĭmark-Sacker (HNS) bifurcation. Let $p, q \in \mathbb{C}^2$ be vectors satisfying the relations

$$Jq = \lambda q, \quad J^\top p = \bar{\lambda} p, \quad \langle p, q \rangle = 1, \tag{5}$$

where $\langle \cdot, \cdot \rangle$ denotes the standard innerproduct on $\mathbb{C}^2$ which is conjugate linear in the *first* component and linear in the *second* component. Define the function

$$H(z, \bar{z}) = \langle p, \mathscr{F}(x_0 + zq + \bar{z}\bar{q}) - x_0 \rangle$$

and consider its Taylor expansion around $(z, \bar{z}) = (0, 0)$:

$$H(z, \bar{z}) = e^{i\theta} z + \sum_{2 \le j+k \le 3} \frac{1}{j!k!} h_{jk} z^j \bar{z}^k + O(|z|^4).$$

The first Lyapunov coefficient is then defined by

$$\ell_1 = \mathrm{Re}\left(\frac{e^{-i\theta} h_{21}}{2} - \frac{(1 - 2e^{i\theta}) e^{-2i\theta}}{2(1 - e^{i\theta})} h_{20} h_{11} \right) - \frac{1}{2}|h_{11}|^2 - \frac{1}{4}|h_{02}|^2. \tag{6}$$

Theorem 4.6 of Kuznetsov [2004] implies that if $\ell_1 < 0$ then the HNS bifurcation is supercritical, which means that a unique stable, closed invariant curve is born as the fixed point loses stability. Note that for maps with only quadratic nonlinear terms we always have that $h_{21} = 0$ which leads to a simplification of the expression for ℓ_1.

If J is a *real* 2×2 matrix, then the vectors $p, q \in \mathbb{C}^2$ satisfying equation (5) can be chosen as

$$q = \begin{pmatrix} a_{12} \\ e^{i\theta} - a_{11} \end{pmatrix}, \quad p = \frac{1}{a_{12}a_{21} + (e^{-i\theta} - a_{11})^2} \begin{pmatrix} a_{21} \\ e^{-i\theta} - a_{11} \end{pmatrix}, \tag{7}$$

or, alternatively as

$$q = \begin{pmatrix} e^{i\theta} - a_{22} \\ a_{21} \end{pmatrix}, \quad p = \frac{1}{(e^{-i\theta} - a_{22})^2 + a_{12}a_{21}} \begin{pmatrix} e^{-i\theta} - a_{22} \\ a_{12} \end{pmatrix}. \tag{8}$$

2.2 The Hopf-Neĭmark-Sacker bifurcation

The following three results confirm what is already suggested by the Lyapunov diagrams of Figures 1–3: along a curve in the parameter plane a stable fixed point bifurcates through a Hopf-Neĭmark-Sacker (HNS) bifurcation.

Proposition 1 (HNS bifurcation of the predator-prey map)**.** *The predator-prey map $\mathscr{P}$ has a fixed point $(\frac{1}{b}, 1 - \frac{1}{a} - \frac{1}{b})$ which is stable if and only if*

$$1 < a < 9 \quad \textit{and} \quad \max\left\{ \frac{a}{a-1}, \frac{3a}{a+3} \right\} < b < \frac{2a}{a-1}.$$

Along the curve $b = 2a/(a-1)$ the fixed point loses stability through a supercritical HNS bifurcation and gives birth to a unique stable, closed invariant circle. The strong resonances are located at the values $a \in \{1, 5, 7, 9\}$.

Proof. Evaluating the Jacobian matrix of the map $\mathscr{P}$ at the fixed point $(\frac{1}{b}, 1-\frac{1}{a}-\frac{1}{b})$ gives

$$J = \begin{pmatrix} 1-a/b & -a/b \\ b-b/a-1 & 1 \end{pmatrix},$$

which implies that $\det(J) = a - 2a/b$ and $\mathrm{tr}(J) = 2 - a/b$. From equation (4) it follows that the fixed point is stable if and only if the inequalities

$$1 < a < 9 \quad \text{and} \quad \max\left\{\frac{a}{a-1}, \frac{3a}{a+3}\right\} < b < \frac{2a}{a-1}$$

are satisfied. Along the curve $b = 2a/(a-1)$ the fixed point loses stability as a complex conjugate pair of eigenvalues crosses the unit circle with nonzero speed. At the HNS bifurcation the eigenvalues are given by

$$\lambda_\pm = \frac{5-a \pm i\sqrt{16-(5-a)^2}}{4} = e^{\pm i\theta} \quad \text{where} \quad \tan\theta = \frac{\sqrt{16-(5-a)^2}}{5-a}. \tag{9}$$

Strong resonances occur when $\lambda_\pm = 1$ (1:1 resonance), $\lambda_\pm = -1$ (1:2 resonance), $\lambda_\pm = -\frac{1}{2} \pm \frac{1}{2}\sqrt{3}i$ (1:3 resonance), and $\lambda = \pm i$ (1:4 resonance). From equation (9) it follows that these values of $\lambda_\pm$ are attained at $a = 1$, $a = 9$, $a = 7$ and $a = 5$, respectively.

We use equation (8) with $a_{22} = 1$, $a_{21} = 1$, and $a_{12} = (1-a)/2$. Computations with the computer algebra package Mathematica Wolfram Research, Inc. [2016] then gives the following normal form coefficients:

$$\begin{aligned} h_{20} &= \frac{-4a + 8ae^{i\theta} - 8ae^{2i\theta} + 4ae^{3i\theta}}{-3 + a + 4e^{i\theta} - 2e^{2i\theta}}, \\ h_{11} &= \frac{-4a + 10ae^{i\theta} - 8ae^{2i\theta} + 2ae^{3i\theta}}{(3-a)e^{i\theta} - 4e^{2i\theta} + 2e^{3i\theta}}, \\ h_{02} &= \frac{8a - 12ae^{-i\theta} + 4ae^{-2i\theta}}{3 - a - 4e^{i\theta} + 2e^{2i\theta}}, \\ h_{21} &= 0. \end{aligned}$$

The expression of the first Lyapunov coefficient is rather complicated and will therefore be omitted. Figure 5 shows a graph of ℓ_1 as a function of the parameter a. Indeed, $\ell_1 < 0$ for $1 < a < 9$. This completes the proof. □

Proposition 2 (HNS bifurcation of the Lorenz map)**.** *The Lorenz map $\mathscr{L}$ has two fixed points $(\pm\sqrt{\alpha}, \alpha)$ which are stable when*

$$\alpha > 0 \quad \textit{and} \quad 0 < \tau < \min\left\{\frac{1-\sqrt{1-8\alpha}}{2\alpha}, \frac{1}{2\alpha}\right\}.$$

Along the curve $\tau = 1/2\alpha$ both fixed points lose stability through a supercritical HNS bifurcation which gives birth to a pair *of coexisting stable invariant circles. The strong resonances are located at the values $\alpha \in \{\frac{1}{4}, \frac{1}{6}, \frac{1}{8}\}$.*

Proof. Evaluating the Jacobian matrix of the map $\mathscr{L}$ at the fixed points $(\pm\sqrt{\alpha}, \alpha)$ is given by

$$J = \begin{pmatrix} 1 & \mp\tau\sqrt{\alpha} \\ \pm 2\tau\sqrt{\alpha} & 1-\tau \end{pmatrix},$$

which implies that $\det(J) = 1 - \tau + 2\alpha\tau^2$ and $\mathrm{tr}(J) = 2 - \tau$. From equation (4) it follows that a sufficient condition for stability of the fixed points is given by

$$\alpha > 0 \quad \text{and} \quad 0 < \tau < \min\left\{\frac{1-\sqrt{1-8\alpha}}{2\alpha}, \frac{1}{2\alpha}\right\}.$$

Along the curve $\tau = (1 - \sqrt{1-8\alpha})/2\alpha$ the fixed points lose stability as one eigenvalue passes -1. The eigenvalues become complex along the line $\alpha = \frac{1}{8}$. Along the curve $\tau = 1/2\alpha$, where $\alpha > \frac{1}{8}$, the fixed points lose stability through a complex conjugate pair of eigenvalues crossing the unit circle with nonzero speed. At the HNS bifurcation the eigenvalues are given by

$$\lambda_\pm = \frac{4\alpha - 1 \pm i\sqrt{8\alpha - 1}}{4\alpha} = e^{\pm i\theta} \quad \text{where} \quad \tan\theta = \frac{\sqrt{8\alpha-1}}{4\alpha - 1}. \tag{10}$$

Strong resonances occur when eigenvalues $\lambda_\pm = 1$ (1:1 resonance), $\lambda_\pm = -1$ (1:2 resonance), $\lambda_\pm = -\frac{1}{2} \pm \frac{1}{2}\sqrt{3}i$ (1:3 resonance), and $\lambda = \pm i$ (1:4 resonance). From equation (10) it follows that the 1:1 resonance does not occur. The remaning strong resonances occur for the values $\alpha = \frac{1}{8}$, $\alpha = \frac{1}{6}$, and $\alpha = \frac{1}{4}$, respectively.

We use equation (7) with $a_{11} = 1$, $a_{12} = -1/2\sqrt{\alpha}$, and $a_{21} = 1/\sqrt{\alpha}$. Computations with the computer algebra package Mathematica then gives the following normal form coefficients:

$$h_{20} = \frac{-3 + 3e^{i\theta}}{-2\alpha + 4\alpha^2 - 8\alpha^2 e^{i\theta} + 4\alpha^2 e^{2i\theta}},$$

$$h_{11} = \frac{-3 + e^{-i\theta} + 2e^{i\theta}}{-2\alpha + 4\alpha^2 - 8\alpha^2 e^{i\theta} + 4\alpha^2 e^{2i\theta}},$$

$$h_{02} = \frac{-3 + 2e^{-i\theta} + e^{i\theta}}{-2\alpha + 4\alpha^2 - 8\alpha^2 e^{i\theta} + 4\alpha^2 e^{2i\theta}},$$

$$h_{21} = 0.$$

The expression of the first Lyapunov coefficient is rather complicated and will therefore be omitted. Figure 6 shows a graph of ℓ_1 as a function of the parameter α. Indeed, $\ell_1 < 0$ for $\frac{1}{8} < \alpha$. This completes the proof. □

Proposition 3 (HNS bifurcation of the fold-and-twist map)**.** *For $0 < \varphi < 2\pi$ the map $\mathscr{T}$ has a fixed point $(\frac{2-a}{2a}, -\frac{2-a}{2a}\cot\frac{1}{2}\varphi)$ which loses stability through a supercritical HNS bifurcation along the line $a = 3$ and gives birth to a unique stable, closed invariant circle. The strong resonances are located at the values $\varphi \in \{\pi/2, 2\pi/3, \pi\}$.*

Proof. Evaluating the Jacobian matrix of the map $\mathscr{T}$ at the fixed point $(\frac{2-a}{2a}, -\frac{2-a}{2a}\cot\frac{1}{2}\varphi)$ gives the matrix

$$J = \begin{pmatrix} (a-2)\cos\varphi & -\sin\varphi \\ (a-2)\sin\varphi & \cos\varphi \end{pmatrix},$$

which implies that $\det(J) = a - 2$ and $\mathrm{tr}(J) = (a-1)\cos\varphi$. From equation (4) it follows that the fixed point is stable if and only if $1 < a < 3$. Along the line $a = 3$ the fixed point loses stability as a complex conjugate pair of eigenvalues crosses the unit circle with nonzero speed. At the HNS bifurcation the eigenvalues are simply given by $\lambda_\pm = e^{\pm i\varphi}$. It immediately follows that the strong resonances occur for $\varphi \in \{\pi/2, 2\pi/3, \pi\}$.

We use equation (7) with $a_{11} = \cos\varphi$, $a_{12} = -\sin\varphi$, and $a_{21} = \sin\varphi$. Computations with the computer algebra package Mathematica then gives the following normal form coefficients:

$$h_{20} = 3e^{i\varphi}\sin\varphi, \quad h_{11} = 3e^{i\varphi}\sin\varphi, \quad h_{02} = 3e^{i\varphi}\sin\varphi, \quad h_{21} = 0,$$

so that the first Lyapunov coefficient is given by

$$\ell_1 = -\frac{27}{2}\sin^2\varphi.$$

Clearly, $\ell_1 < 0$ for $0 < \varphi < \pi$. This completes the proof. □

Along each HNS bifurcation curve the eigenvalues of a fixed point are of the form $e^{\pm i\theta}$. At points where $\theta = p/q$ is rational so-called resonance tongues of order p:q emanate. These are indeed clearly visible in the Lyapunov diagrams of Figures 1–3. The boundaries of these tongues are formed by two saddle-node bifurcations, and for parameter values within a tongue a stable periodic point coexists with a saddle periodic point. The unstable manifold of the saddle periodic point forms an invariant circle. For the 1:5 resonance

tongue of the map $\mathscr{P}$ such an invariant circle is shown in Figure 7. The invariant circles of the maps $\mathscr{L}$ and $\mathscr{T}$ are qualitatively similar and hence not shown. The points along the bifurcation curve for which $\theta \in \{2\pi, \pi, 2\pi/3, \pi/2\}$ are so-called strong resonances. For such parameter values more than one closed invariant curve can appear, or such a curve may not exist at all [Kuznetsov, 2004].

Upon parameter variation, the invariant circle can be destroyed by homoclinic tangencies between the stable and unstable manifolds of the unstable periodic point, or the circle can interact with other objects via heteroclinic tangencies. This scenario will not be considered in the present paper, but see Broer et al. [1993, 1998] for an extensive discussion. Instead, we will focus on chaotic dynamics arising through bifurcations of the periodic points in the resonance tongues.

3 Folding and chaotic dynamics

In this section we discuss the implications of the non-invertible nature of the three maps. We will discuss Hénon-like attractors and their folded structure. In addition, we discuss the existence of snap-back repellers which is also a consequence of non-invertibility.

3.1 Critical lines

An important tool in the study of non-invertible planar maps is the so-called critical manifold Mira et al. [1994, 1996]. For a smooth map $\mathscr{F} : \mathbb{R}^2 \to \mathbb{R}^2$ we define the set

$$LC_{-1} = \{(x, y) \in \mathbb{R}^2 \, : \, \det D\mathscr{F}(x, y) = 0\}.$$

The critical line LC (in French: "ligne critique") is then defined as the image of LC_{-1} under the map $\mathscr{F}$. The critical line LC and its iterates play an important role in the bifurcations of basin boundaries and in bounding invariant regions. The critical line for the maps studied in this work are given by the following propositions. These results follow in a straightforward manner from the definitions given above, and therefore their proofs are omitted.

Proposition 4 (Critical line of the predator-prey map)**.** *For the map $\mathscr{P}$ the critical line*

and its inverse image are given by the equations

$$\begin{aligned} LC_{-1} &: x = \tfrac{1}{2}, \\ LC &: bx + ay = \tfrac{1}{4}ab. \end{aligned}$$

Proposition 5 (Critical line of the Lorenz map)**.** *For the map $\mathscr{L}$ with $\tau > 0$ and $\tau \neq 1$ the critical line and its inverse image are given by the equations*

$$\begin{aligned} LC_{-1} &: y = \frac{1+\alpha\tau}{\tau} + \frac{2\tau x^2}{1-\tau}, \\ LC &: \left(y - \frac{(1-\tau)(1+\alpha\tau)}{\tau} \right)^3 = \frac{27(1-\tau)^2 x^2}{4\tau}. \end{aligned}$$

If $\tau = 1$ then LC_{-1} is given by the line $x = 0$ so that LC reduces to the single point $(0, 0)$.

Proposition 6 (Critical line of the fold-and-twist map)**.** *For the map $\mathscr{T}$ the critical line and its inverse image are given by the equations*

$$\begin{aligned} LC_{-1} &: x = 0, \\ LC &: x\cos\varphi + y\sin\varphi = \tfrac{1}{4}(a-2). \end{aligned}$$

Now consider any smooth, noninvertible map $\mathscr{F} : \mathbb{R}^2 \to \mathbb{R}^2$. Under general conditions the set LC_{-1} is a smooth curve in $\mathbb{R}^2$. A sufficient condition for this is, for example, that 0 is a regular value of the map $(x, y) \mapsto \det D\mathscr{F}(x, y)$. This is indeed the case for the maps $\mathscr{P}$, $\mathscr{L}$, and $\mathscr{T}$. Assume that LC_{-1} is parameterized with $\lambda : I \to \mathbb{R}^2$, where I is an open interval around 0. Now let $\gamma : I \to \mathbb{R}^2$ be any other smooth curve that intersects the curve $LC_{-1} = \lambda$. Without loss of generality we may assume that $\gamma(0) = \lambda(0)$. The vectors $\gamma'(0)$ and $\lambda'(0)$ are the tangent vectors to the curves γ and λ at their point of intersection.

The image $\mathscr{F}(\lambda)$ is by definition the critical line LC. Note that the image $\mathscr{F}(\gamma)$ may have self-intersections due to the noninvertibility of $\mathscr{F}$. Away from such self-intersections $\mathscr{F}(\gamma)$ is again a smooth curve which intersects the critical line LC at the point $\mathscr{F}(\gamma(0)) = \mathscr{F}(\lambda(0))$. The tangent vectors at this point are given by $D\mathscr{F}(\gamma(0))\gamma'(0)$ and $D\mathscr{F}(\lambda(0))\lambda'(0)$. Since $\gamma(0) = \lambda(0) \in LC_{-1}$ it follows that the matrix $D\mathscr{F}(\gamma(0))$ has rank 1 which means that the vectors $D\mathscr{F}(\gamma(0))\gamma'(0)$ and $D\mathscr{F}(\lambda(0))\lambda'(0)$ are parallel. This implies that the curve $\mathscr{F}(\gamma)$ is *tangent* to LC at $\mathscr{F}(\gamma(0))$. An exception to this situation is when the vector $\gamma'(0)$ belongs to the null space of $D\mathscr{F}(\gamma(0))$ in which case $\mathscr{F}(\gamma)$ has a *cusp* point intersection with LC. These two cases are illustrated for the fold-and-twist map $\mathscr{T}$ with $(a, \varphi) = (3.2, 2\pi/5)$ in Figures 8 and 9.

3.2 Routes to chaos and Hénon-like attractors

In this section we investigate the routes to chaos and the structure of chaotic attractors for the three maps. The discussion will be restricted to resonance tongues of order 1:4, 1:5, and 2:5 since these tongues are the largest in the parameter plane in the sense of Lebesgue measure. Near other tongues we expect similar dynamical behavior.

Near a HNS bifurcation a resonance tongue contains a pair of stable and unstable periodic points. The stable periodic point is either a node (real eigenvalues) or a focus (complex eigenvalues). Periodic points of focus type typically bifurcate through a secondary HNS bifurcation, which leads to a new set of resonance tongues. The newly created periodic points in these secondary tongues can undergo period-doubling bifurcations or HNS bifurcations. For this reason we restrict the discussion to the primary resonance tongues in which the stable periodic point is a node.

The periodic points of node type typically undergo a period-doubling cascade upon parameter variation. This is illustrated by means of Lyapunov diagrams for the maps $\mathscr{P}$, $\mathscr{L}$, and $\mathscr{T}$ in Figures 10–12. Period doubling cascades lead to the creation of infinitely many unstable periodic points. These points play a key role in the formation of chaotic attractors in two different ways. One scenario is that a periodic point of source type becomes a so-called *snap-back repeller*, which provides a sufficient condition for chaotic dynamics. We will discuss snap-back repellers in more detail in Section 3.3.

Another scenario is that a periodic point of saddle type has an unstable manifold which shows a strong resemblance to the chaotic attractor observed for the same parameter values. Such attractors will be referred to as *Hénon-like* attractors. Numerical evidence of Hénon-like attractors for the maps $\mathscr{P}$ (in the 1:5 tongue), $\mathscr{L}$ (in the 1:4 tongue), and $\mathscr{T}$ (in the 2:5 tongue) is presented in Figures 13–15. Each figure shows a chaotic attractor together with the unstable manifold of a saddle periodic point. Due to the striking resemblance we conjecture that each chaotic attractor shown is in fact the closure of an unstable manifold of the saddle point.

Note that strictly speaking, we must speak of an "unstable set" instead of an "unstable manifold". Indeed, since the maps $\mathscr{P}$, $\mathscr{L}$, and $\mathscr{T}$ are not diffeomorphisms the unstable set can have self-intersections which are indeed clearly visible in the aforementioned figures. An explanation of this phenomenon is already provided in Section 3.1 where it is shown that the image of any curve under a noninvertible map may have self-intersections. Figure

16 shows a close up of the Hénon-like attractor of Figure 13 together with iterates of the critical line LC. Clearly, the unstable manifolds forms tangencies along the iterates of LC. Observe that LC is described by a linear equation and its iterate is an algebraic curve of degree 2. Therefore, the n-th iterate of LC is an algebraic curve of degree 2^n. Hence, iterates of LC become very complex and so do the foldings of the unstable manifolds.

3.3 Snap-back repellers

In his 1989 paper, in which the map $\mathscr{L}$ was introduced, Lorenz pointed out the following sufficient condition for a non-invertible map to exhibit sensitive dependence on initial conditions: if the map has an attractor containing two distinct points which are mapped to the same point, then the map exhibits sensitive dependence on initial conditions. Lorenz only provided a heuristic argument and suggested that his observation is part of mathematical folklore. However, already in 1978 Marotto proved a theorem in this spirit that provides a sufficient condition for chaotic dynamics of multi-dimensional maps. In what follows $\|\cdot\|$ denotes the standard Euclidean norm on $\mathbb{R}^n$ and $B_r(p) := \{x \in \mathbb{R}^n : \|x - p\| \leq r\}$ denotes a closed ball with radius r around the point p.

Definition 1 (Marotto 1978, 2005)**.** *Let $\mathscr{F} : \mathbb{R}^n \to \mathbb{R}^n$ be a differentiable map. A fixed point p of $\mathscr{F}$ is called a* snap-back repeller *if the following two conditions are satisfied:*

(i) the fixed point p is expanding*, which means that there exists an $r > 0$ such that the eigenvalues of $D\mathscr{F}(x)$ exceed 1 in absolute value for all $x \in B_r(p)$;*

(ii) there exists a point $x_0 \in B_r(p)$ with $x_0 \neq p$ and $m \in \mathbb{N}$ such that $x_m = p$ and $\det(D\mathscr{F}(x_k)) \neq 0$ for all $1 \leq k \leq m$ where $x_k = \mathscr{F}^k(x_0)$.

Theorem 1 (Marotto 1978)**.** *If $\mathscr{F} : \mathbb{R}^n \to \mathbb{R}^n$ has a snap-back repeller, then $\mathscr{F}$ is chaotic in the sense of Marotto. That is, there exist*

(i) $N \in \mathbb{N}$ such that for each $p \geq N$ the map $\mathscr{F}$ has a periodic point of period p;

(ii) a scrambled set *for $\mathscr{F}$, i.e., an uncountable set S containing no periodic points such that*

(a) $\mathscr{F}(S) \subset S$,

(b) for every $x, y \in S$ with $x \neq y$ we have

$$\limsup_{k\to\infty} \|\mathscr{F}^k(x) - \mathscr{F}^k(y)\| > 0,$$

(c) for every $x \in S$ and any periodic point y we have

$$\limsup_{k\to\infty} \|\mathscr{F}^k(x) - \mathscr{F}^k(y)\| > 0,$$

(d) an uncountable subset S_0 of S such that for every $x, y \in S_0$ we have

$$\limsup_{k\to\infty} \|\mathscr{F}^k(x) - \mathscr{F}^k(y)\| = 0.$$

Of course, invertible maps cannot have snap-back repellers. For these maps the occurrence of chaotic dynamics is often proved via the existence of bifurcations that lead to homoclinic tangencies of stable and unstable manifolds of periodic points of saddle type, see Palis and Takens [1993] for a general account. Marotto's theorem provides a sufficient condition for chaotic dynamics of non-invertible maps based on expanding periodic points and circumvents the computation of stable and unstable manifolds and their intersections. In this sense proving the occurrence of chaotic dynamics for noninvertible maps is easier than for invertible maps. Note that the existence of a snap-back repeller does not reveal the *structure* of a chaotic attractor. Below we will give numerical evidence of a snap-back repeller that coexists with a saddle periodic point giving rise to a Hénon-like attractor.

The following theorem, of which the proof is based on the implicit function theorem, will be useful to prove the existence of snap-back repellers for a range of parameters of the fold-and-twist map $\mathscr{T}$.

Theorem 2 (Li & Lyu 2009)**.** *Denote by $\|\cdot\|$ and $\|\cdot\|_{\mathrm{op}}$ the Euclidean norm and the induced operator norm, respectively. Let $\mathscr{F} : \mathbb{R}^n \to \mathbb{R}^n$ be a C^1 map with a snap-back repeller. If $\mathscr{G} : \mathbb{R}^n \to \mathbb{R}^n$ is a C^1 map such that $\|\mathscr{F} - \mathscr{G}\| + \|D\mathscr{F} - D\mathscr{G}\|_{\mathrm{op}}$ is sufficiently small, then $\mathscr{G}$ has a snap-back repeller.*

The concept of snap-back repellers is not new, but it is still the subject of intensive study. Some works that appeared in the last ten years are [Chen et al., 2016, Peng, 2007, Ren et al., 2017, Salman et al., 2016, Shi and Yu, 2008, Yuan et al., 2011, Zhao and Li, 2016]. Note that differentiability of the map is an essential condition for Theorem 1, but see Gardini and Tramontana [2010a,b] for results which do not require smoothness.

3.3.1 Existence of snap-back repellers for the map $\mathscr{T}$

In this section we prove the existence of snap-back repellers for the map $\mathscr{T}$ in the special case $\varphi = \pi/2$. First note that for this parameter value the periodic point born at the HNS bifurcation described in Proposition 3 can be computed explicitly.

Proposition 7. *For $\varphi = \pi/2$ and $a > 3$ the fold-and-twist map $\mathscr{T}$ has three period-4 points which are given by $(-p_1, p_3)$, $(-p_2, p_3)$, and $(-p_4, p_4)$, where*

$$p_1 = -\frac{1}{2}, \quad p_2 = \frac{a-2}{2a}, \quad p_3 = \frac{1+\sqrt{(a-3)(a+1)}}{2a}, \quad p_4 = \frac{1-\sqrt{(a-3)(a+1)}}{2a}.$$

The points $(-p_1, p_3)$ and $(-p_2, p_3)$ are unstable. The point $(-p_4, p_4)$ is stable for $3 < a < 1+\sqrt{6}$, but loses stability at $a = 1+\sqrt{6}$ as two Floquet multipliers pass through -1. At $a = 3$ all three period-4 points coalesce with a fixed point.

Proof. Recall that $f(x) = \frac{1}{4}(a-2) - ax^2$. For $\varphi = \pi/2$ we have $\mathscr{T}(x, y) = (-y, f(x))$ so that $\mathscr{T}^4(x, y) = (-f^2(x), f^2(y))$. Hence, (x, y) is a period-4 point of $\mathscr{T}$ if and only if $-x$ and y are fixed points of f^2. For $3 < a < 4$ the fixed points for f^2 are given by $p_1, \ldots, p_4$. This implies that there are 16 candidates for a period-4 point of $\mathscr{T}$ which are given by $(-p_i, p_j)$ for $1 \le i, j \le 4$. Straightforward computations show that:

- $(-p_1, p_1)$ and $(-p_2, p_2)$ are unstable fixed points;
- $(-p_1, p_2) \mapsto (-p_2, p_1)$ is an unstable period-2 orbit;
- $(-p_1, p_3) \mapsto (-p_3, p_1) \mapsto (-p_1, p_4) \mapsto (-p_4, p_1)$ is a period-4 orbit;
- $(-p_2, p_3) \mapsto (-p_3, p_2) \mapsto (-p_2, p_4) \mapsto (-p_4, p_2)$ is a period-4 orbit;
- $(-p_4, p_4) \mapsto (-p_4, p_3) \mapsto (-p_3, p_3) \mapsto (-p_3, p_4)$ is a period-4 orbit.

This exhausts all period-4 orbits. The Floquet multipliers of a period-4 point $(-p_i, p_j)$ are given by $\lambda_1 = 4a^2 p_i f(p_i)$ and $\lambda_2 = 4a^2 p_j f(p_j)$. This implies the following conclusions:

- $(-p_1, p_3)$ has Floquet multipliers $\lambda_1 = a^2$ and $\lambda_2 = 1 - (a-3)(a+1)$, and since $a > 3$ this point is unstable;
- $(-p_2, p_3)$ has Floquet multipliers $\lambda_1 = (2-a)^2$ and $\lambda_2 = 1 - (a-3)(a+1)$, and since $a > 3$ this point is unstable;

- $(-p_4, p_4)$ has Floquet multipliers $\lambda_1 = \lambda_2 = 1 - (a-3)(a+1)$. Note that $|\lambda_{1,2}| < 1$ for $3 < a < 1 + \sqrt{6}$, and at $a = 1 + \sqrt{6}$ both multipliers pass through -1.

This completes the proof. □

We now prove that p_4 is a snap-back repeller for f^2 when $a = 4$. Next, we use this result to show that $(-p_4, p_4)$ is a snap-back repeller for $\mathscr{T}^4$.

Lemma 1. *For $1 + \sqrt{6} < a \leq 4$ the point $p = \left(1 - \sqrt{(a+1)(a-3)}\right)/2a$ is an expanding fixed point of the second iterate of the map $f(x) = \frac{1}{4}(a-2) - ax^2$.*

Proof. Let $g = f^2$, then $g(p) = p$. Note that $g'(x) = -4a^3x^3 + a^2(a-2)x$ has a local minimum at $m = -\sqrt{(a-2)/12a}$. It is straightforward to verify that $g'(m)$ is a decreasing function of a and that $g'(m) = -1$ for $a = 3$. Since $g'(-\frac{1}{2}) = a^2 > 0$ and $g'(0) = 0$ it follows from the intermediate value theorem that for $a > 3$ there exist numbers $-\frac{1}{2} < \xi < m < \eta < 0$ such that $g'(x) = -1$ for $x = \xi$ and $x = \eta$. Hence, $g'(x) < -1$ for all $x \in U := (\xi, \eta)$. For $a = 1 + \sqrt{6}$ we have that $p = \xi = (1 - \sqrt{2})/(2 + 2\sqrt{6})$ so that the point p lies on the boundary of U. For $1 + \sqrt{6} < a \leq 4$ the point p is contained in U. In this case the ball $B_r(p)$ with $r < \min\{|p - \xi|, |p - \eta|\}$ is a repelling neighborhood of p. □

Lemma 2. *For $a = 4$ the second iterate of the map $f(x) = \frac{1}{4}(a-2) - ax^2$ has a snap-back repeller.*

Proof. Let $a = 4$ and define $g(x) = f^2(x) = -\frac{1}{2} + 16x^2 - 64x^4$. Lemma 1 shows that $p = (1 - \sqrt{5})/8$ is an expanding fixed point of g. Hence, there exists $r > 0$ such that $|g'(x)| > 1$ for all $x \in B_r(p)$. Set $x_1 = -p$ so that $g(x_1) = p$. Consider the sequence $x_{k+1} = h(x_k)$ where

$$h(x) = -\tfrac{1}{4}\sqrt{2 - \sqrt{2 - 4x}}$$

is one of the four branches of the multi-valued inverse of g. Since h is strictly decreasing we have that $I := h([-\frac{1}{2}, \frac{1}{2}]) = [-\frac{1}{2\sqrt{2}}, 0]$. Note that h maps I into itself so that $x_k \in I$ for all $k \geq 2$. Since $|h'(x)| < 1$ for all $x \in I$ the mean value theorem shows that $h : I \to I$ is a contractive mapping. Since $p \in I$ is a fixed point of h it follows that $x_k \to p$ as $k \to \infty$. Hence, for $m \in \mathbb{N}$ sufficiently large we have $x_m \in B_r(p)$ and $g^m(x_m) = p$. First note that $g'(x_1) = g'(-p) = 4$, and then observe that for $k \geq 2$ the points x_k lie in the interior of the interval I and $g'(x)$ is only zero at the boundary points of I. Therefore, $g'(x_i) \neq 0$ for all $i = 1, \ldots, m$. □

Proposition 8. *Let $\epsilon > 0$ be sufficiently small. For $4 - \epsilon < a \leq 4$ and $\pi/2 - \epsilon < \varphi < \pi/2 + \epsilon$ the fourth iterate of the fold-and-twist map $\mathscr{T}$ has a snap-back repeller.*

Proof. Note that for $\varphi = \pi/2$ we have $\mathscr{T}(x, y) = (-y, f(x))$ so that $\mathscr{T}^4(x, y) = (-f^2(x), f^2(y))$. Lemma 2 shows that f^2 has a snap-back repeller p in some repelling neighbourhood $(p - r, p + r)$ for $a = 4$. It is straightforward to check that $(-p, p)$ in the neighbourhood $B_r((-p, p))$ is a snap-back repeller for $\mathscr{T}^4$ for $(a, \varphi) = (4, \pi/2)$. Applying the persistence result of Theorem 2 completes the proof. □

3.3.2 Numerical evidence of snap-back repellers

In theory the conditions for a snap-back repeller are easy to verify since the computation of invariant manifolds is circumvented. However, rigorous proofs for the existence of a snap-back repeller are only possible in cases for which the "return time" m in Definition 1 is relatively small. Indeed, if $\mathscr{F} : \mathbb{R}^d \to \mathbb{R}^d$ is a k-to-1 map, then the number of preimages of a fixed point under $\mathscr{F}^m$ is k^m. Therefore, the explicit computation of preimages is only possible for small values of m. In general, it can be expected that when the radius of the repelling neighborhood decreases, a larger number of preimages may be needed in order to return to the neighborhood of the periodic point. Figure 17 illustrates this phenomenon for the map $\mathscr{T}$.

The three maps $\mathscr{P}$, $\mathscr{L}$, and $\mathscr{T}$ all have a fixed point which becomes a source through the HNS bifurcation described in Section 2.2. The numerical evidence presented in Figures 18-20 suggests that for suitable choices of the parameter values the fixed point can become a snap-back repeller. For the three maps we have numerically computed a sequence of preimages by recursively applying the formulas for the inverses presented in Appendix A. Then we checked whether such a preimage returns to an expanding neighborhood ball the fixed point. Note that the number of inverses grows exponentially fast, and for this reason this algorithm is only applicable to snap-back repellers with small "return times".

The period-p points that are born through the HNS bifurcation can also become snap-back repellers for the maps $\mathscr{P}^p$, $\mathscr{L}^p$, and $\mathscr{T}^p$ for suitable parameter values. We consider two different scenario's. In the first scenario a saddle periodic point forming a Hénon-like attractor becomes unstable through a period doubling bifurcation. As an example we consider the map $\mathscr{P}$ in the 1:5 resonance tongue. For $(a, b) = (3.85, 3.2)$ the Hénon-like attractor is shown in Figure 13. Numerical continuation shows that the saddle period-5

point becomes a source due to a period doubling bifurcation at $b \approx 3.404$. At $b = 3.6$ the period-5 points are expanding fixed points of the map $\mathscr{P}$, and in fact they are snap-back repellers. One such snap-back repeller is shown in Figure 21; the remaining four snap-back repellers are not shown.

Another scenario is the coexistence of a saddle periodic point leading to a Hénon-like attractor with a snap-back repeller. As an example we consider the 1:4 resonance tongue for the map $\mathscr{L}$. For $(\alpha, \tau) = (0.28, 2.25)$ the Hénon-like attractor is shown in Figure 14. Within the resonance tongue the saddle period-4 points coexists with a period-4 point which is a source. The numerical evidence of Figure 22 suggests that this point is a snap-back repeller for the map $\mathscr{L}^4$.

3.4 Loss of hyperbolicity

The Lyapunov diagrams of Figures 1–3 suggest that chaotic attractors with two positive Lyapunov exponents occur within sets of positive measure in the parameter plane of each of the maps $\mathscr{P}$, $\mathscr{L}$, and $\mathscr{T}$. It is an interesting question what bifurcation sequences lead to the formation of such attractors and what their geometric structure is. For the map $\mathscr{T}$ the latter question can be answered in the case $\varphi = \pi/2$ since then $\mathscr{T}^2$ is just given by decoupled iterates of the logistic map in the x and y components. This implies that the attractor is simply the Cartesian product of two cantor sets.

The Lyapunov diagrams in Figures 10–12 suggest that the second Lyapunov exponent becomes positive in a continuous manner as a parameter is varied. This phenomenon might be related to loss of hyperbolicity. Abraham and Smale [1970] constructed an example of a map for which dimension of the unstable subspace changes from point to point. The terminology *unstable dimension variability* was coined in Kostelich et al. [1997]. In our maps the following scenario is possible. In a chaotic attractor the unstable periodic points are dense, and upon parameter variation more and more periodic points change from saddles to sources. We will not investigate this in the present paper since this scenario is not specific to non-invertible maps, but for more details see [Alligood and Sander, 2006, Auerbach et al., 1987, Davidchack and Lay, 2000, Dos Santos et al., 2016].

4 Discussion

In this paper we have studied the dynamics of three non-invertible, planar maps. These maps have as common properties that they rotate and fold the plane. It is clear that the maps are *not* related to each other by conjugation. Indeed, the map $\mathscr{L}$ cannot be conjugate to the maps $\mathscr{P}$ and $\mathscr{T}$ due to different number of pre-images. The maps $\mathscr{P}$ and $\mathscr{T}$ cannot be conjugate since otherwise the bifurcation sequences in their 1:5 resonance tongue would be the same.

Despite the lack of conjugacy the three maps share many similarities in both their dynamics and their bifurcations. We have analytically proven the existence of a Hopf–Neĭmark–Sacker bifurcation, which gives rise to resonance tongues in the parameter plane of the map. Inside a resonance tongue a periodic attractor typically either undergoes a period doubling cascade, which leads to chaotic dynamics, or a another Hopf–Neĭmark–Sacker bifurcation, which in turn leads to a new family of tongues. For all maps we have detected chaotic attractors of Hénon-like type: these attractors are conjectured to be the closure of an unstable manifold of a saddle periodic point. Due to the non-invertibility of the map these attractors have a folded structure which can be explained by means of the iterates of the critical line. In addition, we have detected snap-back repellers which may coexist with Hénon-like attractors.

We conjecture that the dynamics described above is typical for planar maps that rotate and fold the plane. We even conjecture that the map $\mathscr{T}$ may serve as a *prototype* for such maps. The advantage of the map $\mathscr{T}$ is that the action of folding and rotation can be controlled separately through the parameters a and φ. In particular, for $\varphi = \pi/2$ we were able to analytically prove the existence of snap-back repellers for the fourth iterate of $\mathscr{T}$. Note that our definition of $\mathscr{T}$ can also be used to consider more complicated non-invertible maps. For example, in (3) we can replace the function $f(x) = \frac{1}{4}(a-2) - ax^2$ by a function that has more than two preimages. A concrete example of such a map could be $f(x) = ax(x^2-1)$. Another choice for f would be the so-called tent map. In this case the fold-and-twist map $\mathscr{F}$ is not smooth, but it may be amenable to a more rigorous investigation. This approach is comparable to the Lozi map that was devised to get a better understanding of the Hénon map. We hope that our map $\mathscr{T}$ with various choices of the map f will inspire other researchers to obtain rigorous theorems for classes of planar, non-invertible maps.

Acknowledgments

The authors would like to express their gratitude to Jan Aarts and Henk Broer for valuable discussions and remarks. The first author has received financial support form the Netherlands Organization for Scientific Research (NWO) in the form of a LION stipend. The first author also thanks Delft University of Technology for hospitality and use of their facilities.

A Preimages of the maps

Preimages of the predator-prey map

Given a point $(u, v) \in \mathbb{R}^2$ we want to find all points (x, y) such that $(u, v) = \mathscr{P}(x, y)$, or equivalently,

$$u = ax(1 - x - y),$$
$$v = bxy.$$

This gives

$$bu + av = abx(1 - x),$$

so that

$$x = \tfrac{1}{2} \pm \sqrt{\tfrac{1}{4} - \tfrac{u}{a} - \tfrac{v}{b}}.$$

After solving for x we find $y = v/bx$.

Preimages of the Lorenz map

Given a point $(u, v) \in \mathbb{R}^2$ we want to find all points (x, y) such that $(u, v) = \mathscr{L}(x, y)$, or equivalently,

$$u = (1 + \alpha\tau)x - \tau xy,$$
$$v = (1 - \tau)y + \tau x^2.$$

From the second equation we obtain $y = (v - \tau x^2)/(1 - \tau)$. Substitution into the first equation then gives the cubic equation $x^3 + px + q = 0$, where

$$p = -\frac{1}{\tau}\left(v - \frac{(1 - \tau)(1 + \alpha\tau)}{\tau}\right), \quad q = -\frac{(1 - \tau)u}{\tau^2},$$

provided that $\tau > 0$. If we know one solution of the cubic equation, say ξ, then a long division gives the quadratic equation $x^2 + \xi x + p + \xi^2 = 0$ by which we can find remaining solutions whenever $-3\xi^2 - 4p \geq 0$. In numerical computations of preimages the initial solution ξ can be found using the Newton-Raphson method.

Preimages of the fold-and-twist map

Given a point $(u, v) \in \mathbb{R}^2$ we want to find all points (x, y) such that $(u, v) = \mathscr{T}(x, y)$, or equivalently,

$$u = f(x)\cos\varphi - y\sin\varphi,$$
$$v = f(x)\sin\varphi + y\cos\varphi.$$

This gives

$$u\cos\varphi + v\sin\varphi = f(x) = \tfrac{1}{4}(a-2) - ax^2,$$

so that

$$x = \pm\sqrt{\frac{a - 2 - 4u\cos\varphi - 4v\sin\varphi}{4a}}.$$

Finally,

$$y = v\cos\varphi - u\sin\varphi.$$

Numerical methods

In this Section we briefly describe the numerical algorithms that we have used to compute Lyapunov exponents and unstable manifolds of saddle points. The algorithms apply to any general smooth map $\mathscr{F} : \mathbb{R}^d \to \mathbb{R}^d$.

Computation of Lyapunov exponents

We estimate Lyapunov exponents using the algorithm described in Benettin et al. [1980a,b]. Given an initial condition we first iterate the map N_{trans} times to obtain a point x_1 on the attractor. Let $u_{1,k}$ denote the k-th standard basis vector of $\mathbb{R}^d$. At each point x_n on the orbit we apply the Jacobian matrix $D\mathscr{F}(x_n)$ to each of the vectors $u_{n,k}$. Each vector tends to align itself along the direction of maximal expansion (or of minimal compression). To prevent the vectors $u_{n,k}$ from collapsing onto one direction the Gram-Schmidt process is used. The average of the logarithms of the rescaling factors then gives an approximation of the k-th Lyapunov exponent.

Let $\langle \cdot, \cdot \rangle$ denote the standard inner product on $\mathbb{R}^d$. For $n \geq 1$ we have applied the following iteration scheme:

$$\begin{aligned} v_{n,k} &= D\mathscr{F}(x_n)u_{n,k}, \\ u_{n,1} &= v_{n,1}, \\ u_{n,k} &= v_{n,k} - \sum_{j=1}^{k-1} \frac{\langle v_{n,k}, u_{n,j} \rangle}{\langle u_{n,j}, u_{n,j} \rangle} u_{n,j}, \\ u_{n+1,k} &= u_{n,k}/\|u_{n,k}\|, \\ x_{n+1} &= \mathscr{F}(x_n). \end{aligned}$$

Iterating this scheme N times then gives the following approximation for the k-th Lyapunov exponent:

$$\lambda_k = \frac{1}{N} \sum_{n=1}^{N} \log \|u_{n,k}\|.$$

Typical values used in our computations are $N_{trans} = 10^3$ and $N = 10^4$.

Computation of unstable manifolds

We compute unstable manifolds of periodic points by means of techniques based on iterating fundamental domains described in [Broer and Takens, 2010, Simó, 1990]. Note that for non-invertible maps the unstable manifold can have self-intersections. Hence the terminology "manifold" is strictly speaking not correct.

Let x be a fixed point of the map $\mathscr{F}$. Assume that the Jacobian matrix $D\mathscr{F}(x)$ has one real eigenvalue $\lambda > 1$ with corresponding eigenvector v and all the other eigenvalues have absolute value strictly smaller than 1. If we want to approximate N points on the manifold, we first compute a linear approximation of the manifold in a small neighborhood of the point x:

$$\begin{aligned} s_j &= \varepsilon \exp(j \log(\lambda^2)/N), \\ w^L_{0,j} &= x - s_j v, \\ w^R_{0,j} &= x + s_j v, \end{aligned}$$

where $j = 1, \ldots, N$. The superscripts L and R indicate the "left" and "right" branch of the manifold, respectively. Then, for $1 \leq k \leq m$ we define inductively

$$\begin{aligned} w^L_{k,j} &= \mathscr{F}(w^L_{k-1,j}), \\ w^R_{k,j} &= \mathscr{F}(w^R_{k-1,j}). \end{aligned}$$

Table 2: Parameters used in the computation of unstable manifolds.

Figure no.	ε	N	m
7	0.001	10	25
13	0.0001	1000	8
14	0.0001	1000	9
15	0.0001	1000	9

The "left" branch of the unstable manifold is then approximated by connecting the points

$$w_{0,1}, \ldots, w_{0,N}, w_{1,1}, \ldots, w_{1,N}, \ldots, w_{m,1}, \ldots, w_{m,N}$$

by line segments. The "right" branch is computed in the same way. For a periodic point x with period p we apply the above procedure with $\mathscr{F}$ replaced by $\mathscr{F}^p$ to each of the points $x, \mathscr{F}(x), \ldots, \mathscr{F}^{p-1}(x)$ along the periodic orbit. Table 2 lists the parameters ε, N, and m that were used to produce our figures.

References

R. Abraham and S. Smale. *Nongenericity of* Ω*-stability*, volume 14 of *Global Analysis, Symp. Pure Math.* American Mathematical Society, 1970.

V. Afraimovich, V. Bykov, and L. Shil'nikov. Origin and structure of the Lorenz attractor. *Akademiia Nauk SSSR Doklady*, 234:336–339, 1977.

K. Alligood and E. Sander. Crossing bifurcations and unstable dimension variability. *Physical Review Letters*, 96:244103, 2006.

D. Auerbach, P. Cvitanović, J.-P. Eckmann, G. Gunaratne, and I. Procaccia. Exploring chaotic motion through periodic orbits. *Physical Review Letters*, 58:2387–2389, 1987.

E. Barreto, B. Hunt, C. Grebogi, and J. Yorke. From high dimensional chaos to stable periodic orbits: the structure of parameter space. *Physical Review Letters*, 78:4561, 1997.

J. Beddington, C. Free, and J. Lawton. Dynamic complexity in predator-prey models framed as difference equations. *Nature*, 255:58–60, 1976.

G. Benettin, L. Galgani, A. Giorgilli, and J.-M. Strelcyn. Lyapunov characteristic exponents for smooth dynamical systems and for Hamiltonian systems; a method for computing all of them. Part 1: theory. *Meccanica*, 15:9–20, 1980a.

G. Benettin, L. Galgani, A. Giorgilli, and J.-M. Strelcyn. Lyapunov characteristic exponents for smooth dynamical systems and for Hamiltonian systems; a method for computing all of them. Part 2: numerical application. *Meccanica*, 15:21–30, 1980b.

H. Broer and F. Takens. *Dynamical Systems and Chaos*, volume 172 of *Applied Mathematical Sciences*. Springer, 2010.

H. Broer, R. Roussarie, and C. Simó. On the Bogdanov-Takens bifurcation for planar diffeomorphisms. In C. Perelló, C. Simó, and J. Solà-Morales, editors, *Equadiff 1991, Proceedings Western European Conference on Differential Equations, Barcelona 1991*, pages 81–92. World Scientific, 1993.

H. Broer, C. Simó, and J. Tatjer. Towards global models near homoclinic tangencies of dissipative diffeomorphisms. *Nonlinearity*, 11:667–770, 1998.

H. Broer, C. Simó, and R. Vitolo. Bifurcations and strange attractors in the Lorenz-84 climate model with seasonal forcing. *Nonlinearity*, 15:1205–1267, 2002.

H. Broer, C. Simó, and R. Vitolo. Quasi-periodic hénon-like attractors in the Lorenz-84 climate model with seasonal forcing. In F. Dumortier, H. Broer, J. Mahwin, A. Vanderbauwhede, and S. Verduyn-Lunel, editors, *Equadiff 2003, Proceedings International Conference on Differential Equations, Hasselt 2003*, pages 714–719. World Scientific, 2005.

H. Broer, C. Simó, and R. Vitolo. Hopf saddle-node bifurcation for fixed points of 3d-diffeomorphisms: Analysis of a resonance 'bubble'. *Physica D*, 237:1773–1799, 2008a.

H. Broer, C. Simó, and R. Vitolo. The Hopf-saddle-node bifurcation for fixed points of 3D-diffeomorphisms: the Arnol′d resonance web. *Bulletin of the Belgian Mathematical Society Simon Stevin*, 15:769–787, 2008b.

H. Broer, C. Simó, and R. Vitolo. Chaos and quasi-periodicity in diffeomorphisms of the solid torus. *Discrete and Continuous Dynamical Systems B*, 14:871–905, 2010.

X. Chen, S. Yuan, Z. Jing, and X. Fu. Bifurcation and chaos of a discrete-time mathematical model for tissue inflammation. *Journal of Dynamics and Difference Equations*, 28:281–299, 2016.

R. Davidchack and Y.-C. Lay. Characterization of transition to chaos with multiple positive Lyapunov exponents by unstable periodic orbits. *Physics Letters A*, 270:308–313, 2000.

V. Dos Santos, J. Szezech Jr., M. Baptista, A. Batista, and I. Caldas. Unstable dimension variability structure in the parameter space of coupled Hénon maps. *Applied Mathematics and Computation*, 286:23–28, 2016.

L. Gardini and F. Tramontana. Snap-back repellers and chaotic attractors. *Physical Review E*, 81:046202, 2010a.

L. Gardini and F. Tramontana. Snap-back repellers in non-smooth functions. *Regular and Chaotic Dynamics*, 15:237–245, 2010b.

S. Garst and A. Sterk. The dynamics of a fold-and-twist map. *Indagationes Mathematicae*, 27:1279–1304, 2016.

J. Guckenheimer and P. Holmes. *Nonlinear oscillations, dynamical systems and bifurcations of vector fields*, volume 42 of *Applied Mathematical Sciences*. Springer, 1983.

J. Guckenheimer and R. Williams. Structural stability of Lorenz attractors. *Publications Mathématiques de l'Institut des Hautes Études Scientifiques*, 50:59–72, 1979.

I. Gumowski and C. Mira. Sur un algorithme de détermination du domaine de stabilité d'un point d'une récurrence non linéaire du deuxième ordre à variables réelles. *Comptes Rendus Acad. Sc. Paris, Série A*, 260:6524–6527, 1965.

I. Gumowski and C. Mira. Sensitivity problems related to certain bifurcations in nonlinear recurrences relations. *Automatica*, 5:303–317, 1969.

E. Kostelich, I. Kan, C. Grebogi, E. Ott, and J. Yorke. Unstable dimension variability: a source of nonhyperbolicity in chaotic systems. *Physica D*, 109:81–90, 1997.

Y. Kuznetsov. *Elements of Applied Bifurcation Theory*, volume 112 of *Applied Mathematical Sciences*. Springer, third edition, 2004.

M.-C. Li and M.-J. Lyu. A simple proof for persistence of snap-back repellers. *Journal of Mathematical Analysis and Applications*, 352:669–671, 2009.

E. Lorenz. Deterministic nonperiodic flow. *Journal of the Atmospheric Sciences*, 20: 130–141, 1963.

E. Lorenz. Computational chaos – a prelude to computational instability. *Physica D*, 35: 299–317, 1989.

F. Marotto. Snap-back repellers imply chaos in $\mathbb{R}^n$. *Journal of Mathematical Analysis and Applications*, 63:199–223, 1978.

F. Marotto. On redefining a snap-back repeller. *Chaos, Solitons and Fractals*, 25:25–28, 2005.

C. Mira. Détermination practique du domaine de stabilité d'un point d'équilibre d'une récurrence non linéaire du deuxième ordre à variables réelles. *Comptes Rendus Acad. Sc. Paris, Série A*, 261:5314–5317, 1964.

C. Mira, D. Fournier-Prunaret, G. L., H. Kawakami, and J. Cathala. Basin bifurcations of two-dimensional non-invertible maps: fractalization of basins. *International Journal of Bifurcations and Chaos*, 4:343–381, 1994.

C. Mira, L. Gardini, A. Barugola, and J. Cathala. *Chaotic Dynamics in Two-Dimensional Noninvertible Maps*. World Scientific Publishing, 1996.

J. Palis and F. Takens. *Hyperbolicity and sensitive chaotic dynamics at homoclinic bifurcations*. Cambridge University Press, 1993.

C.-C. Peng. Numerical computations of orbits and rigorous verification of existence of snapback repellers. *Chaos*, 17:013107, 2007.

J. Ren, L. Yu, and S. Siegmund. Bifurcations and chaos in a discrete predator-prey model with Crowley-Martin functional response. *Nonlinear Dynamics*, 90:19–41, 2017.

S. Salman, A. Yousef, and A. Elsadany. Stability, bifurcation analysis and chaos control of a discrete predator-prey system with square root functional response. *Chaos, Solitons and Fractals*, 93:20–31, 2016.

Y. Shi and P. Yu. Chaos induced by regular snap-back repellers. *Journal of Mathematical Analysis and Applications*, 337:1480–1494, 2008.

C. Simó. On the analytical and numerical continuation of invariant manifolds. In D. Benest and C. Froeschlé, editors, *Modern Methods in Celestial Mechanics*, pages 285–330. Éditions Frontières, 1990.

S. Smale. Differentiable dynamical systems. *Bulletin of the American Mathematical Society*, 73:747–817, 1967.

S. Smale. Finding a horseshoe on the beaches of Rio. *The Mathematical Intelligencer*, 20: 39–44, 1998.

M. Viana. What's new on Lorenz strange attractors? *The Mathematical Intelligencer*, 22 (3):6–19, 2000.

R. Vitolo, H. Broer, and C. Simó. Routes to chaos in the Hopf-saddle-node bifurcation for fixed points of 3D-diffeomorphisms. *Nonlinearity*, 23:1919–1947, 2010.

R. Williams. The structure of the Lorenz attractor. *Publications Mathématiques de l'Institut des Hautes Études Scientifiques*, 50:72–99, 1979.

Wolfram Research, Inc. Mathematica, Version 11.0.1.0, 2016. Champaign, IL, 2016.

S. Yuan, T. Jiang, and Z. Jing. Bifurcations and chaos in the Tinkerbell map. *International Journal of Bifurcations and Chaos*, 21:3137–3156, 2011.

M. Zhao and C. Li. Complex dynamic behaviour of an economic cycle model. *Journal of Difference Equations and Applications*, 22:1777–1790, 2016.

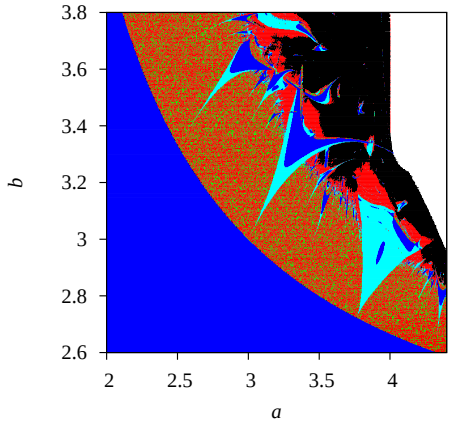

Figure 1: Lyapunov diagram of attractors for the map $\mathscr{P}$ as a function of the parameters a and b. For the color coding see Table 1.

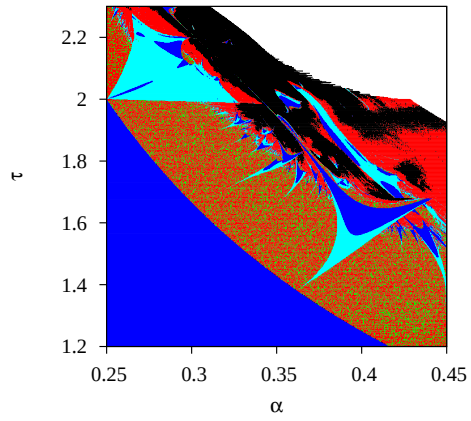

Figure 2: As Figure 1, but for the map $\mathscr{L}$.

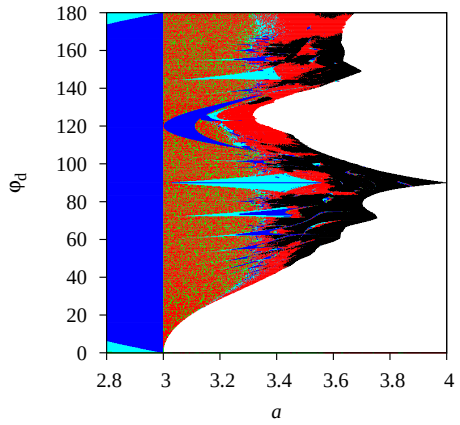

Figure 3: As Figure 1, but for the map $\mathscr{T}$.

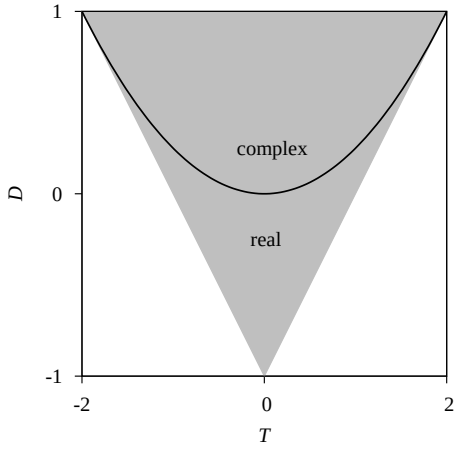

Figure 4: Let T and D respectively denote the trace and determinant of the Jacobian matrix of a map $\mathscr{F}$ evaluated at a periodic point. For values of (T, D) within the grey triangle the periodic point is stable. For $D > T^2/4$ the Floquet multipliers of the periodic point are complex.

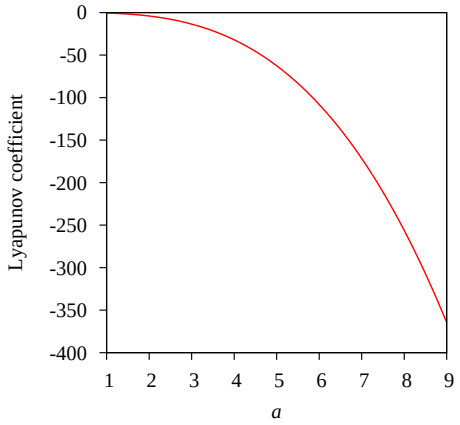

Figure 5: Lyapunov coefficient as a function of the parameter a for the HNS bifurcation of the map $\mathscr{P}$.

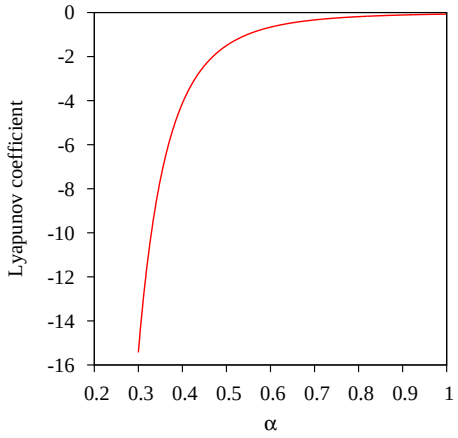

Figure 6: Lyapunov coefficient as a function of the parameter α for the HNS bifurcation of the map $\mathscr{L}$.

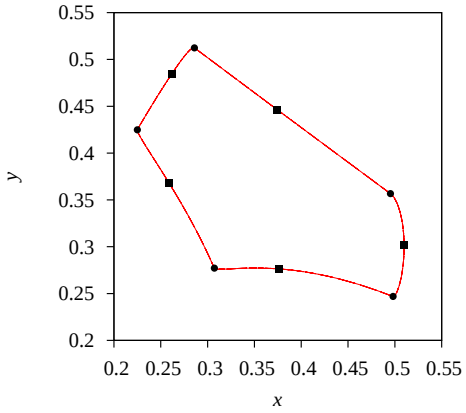

Figure 7: Invariant circle in the 1:5 resonance tongue of the map $\mathscr{P}$ with $(a, b) = (3.9, 2.9)$ formed by the unstable manifolds of the saddle period-5 points (squares). The stable period-5 points are indicated by circles.

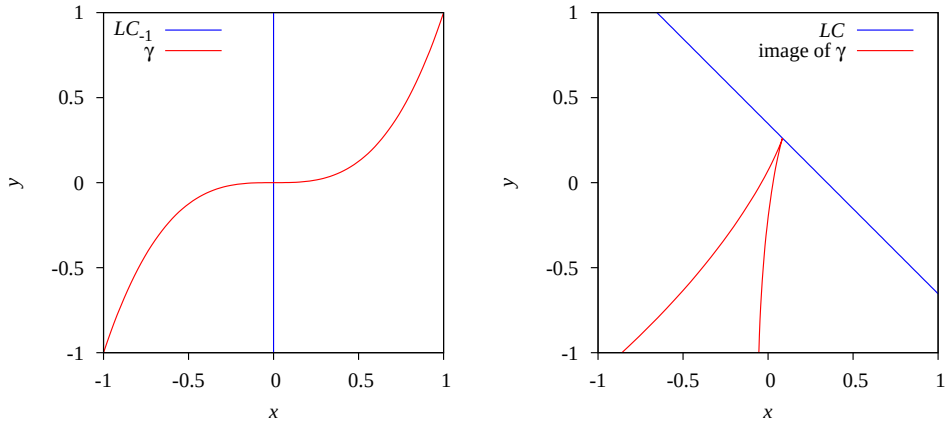

Figure 8: The curve $\gamma(t) = (t, t^3)$ intersects the line LC_{-1}. Its image intersects the line LC in a cusp.

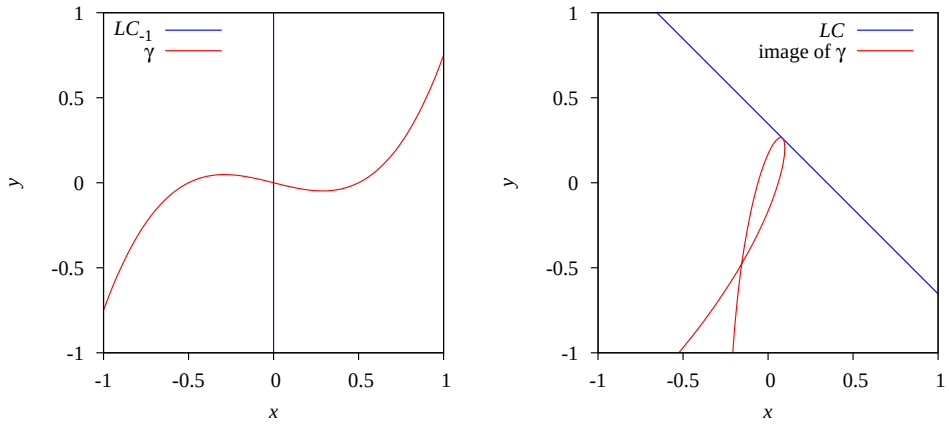

Figure 9: The curve $\gamma(t) = (t, t(t+\frac{1}{2})(t,(t-\frac{1}{2}))$ intersects the line LC_{-1}. Its image is tangent to LC. Note that the image of γ also has a self-intersection.

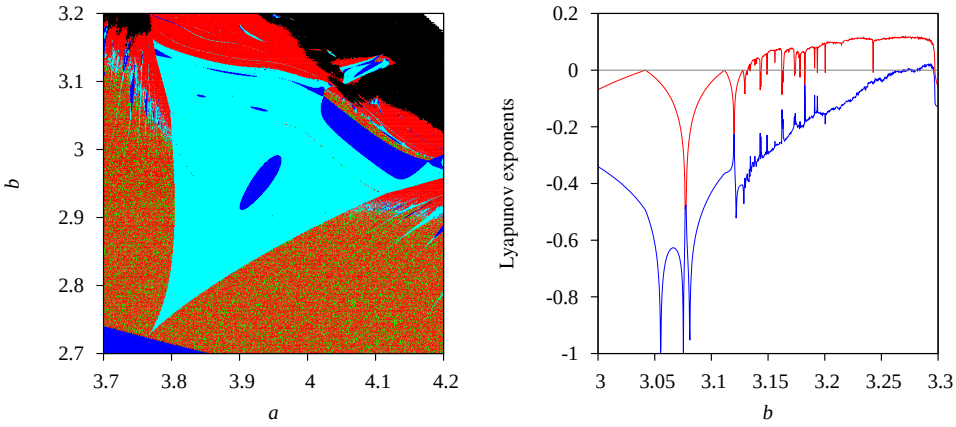

Figure 10: Left panel: 1:5 resonance tongue of $\mathscr{P}$ in the (a, b)-plane. Right panel: Lyapunov exponents as a function of the parameter b while keeping the parameter $a = 3.85$ fixed.

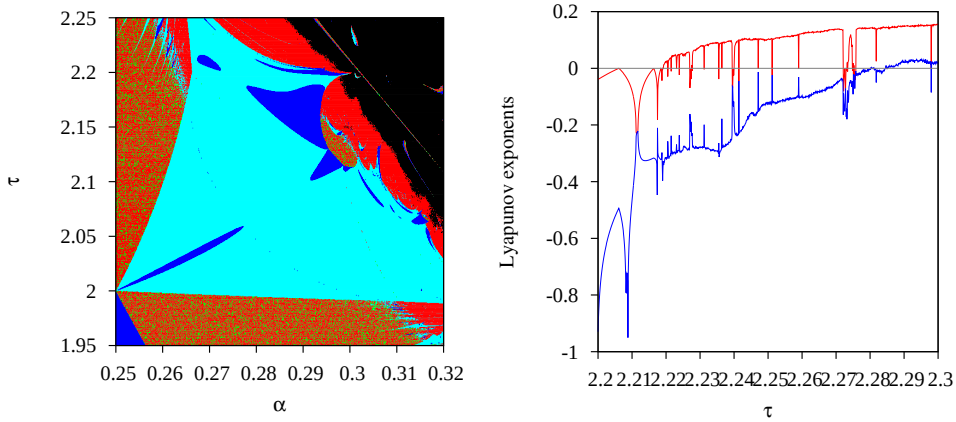

Figure 11: As Figure 10, but for the 1:4 resonance tongue of the map $\mathscr{L}$. In the right panel the parameter $\alpha = 0.28$ is kept fixed.

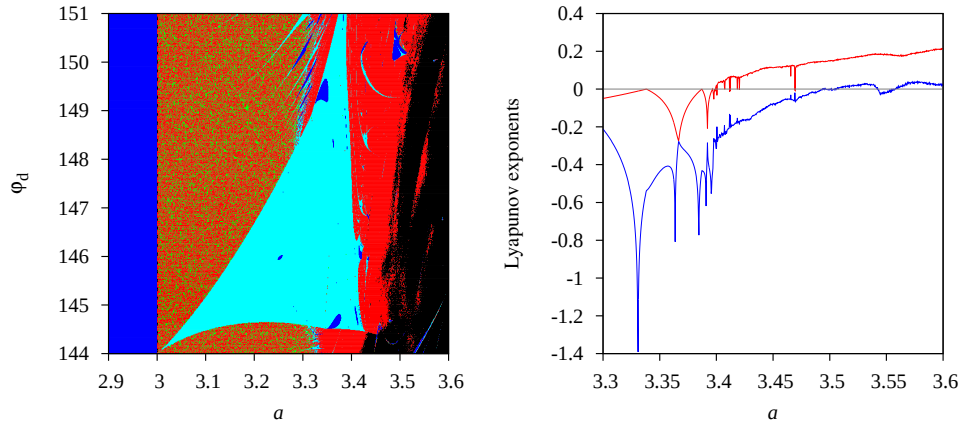

Figure 12: As Figure 10, but for the 2:5 resonance tongue of the map $\mathscr{T}$. In the right panel the parameter $\varphi_d = 148$ is kept fixed.

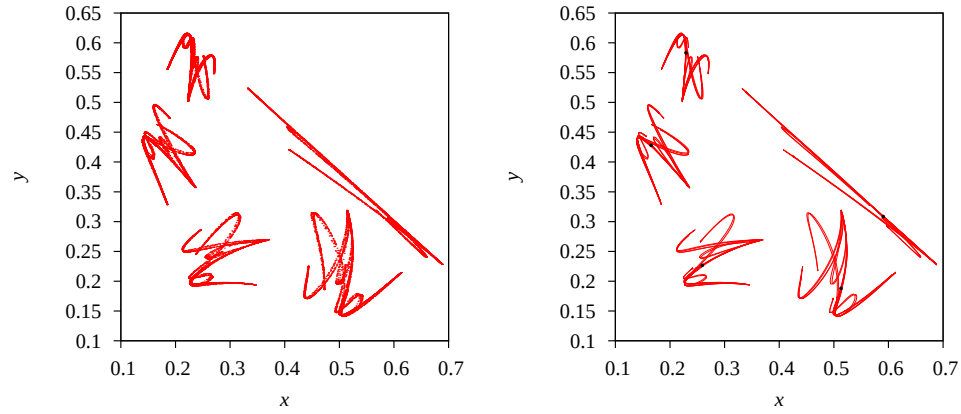

Figure 13: A chaotic attractor of the map $\mathscr{P}$ for $(a, b) = (3.85, 3.2)$ (left panel) and the unstable manifold of a saddle period-5 point (right panel).

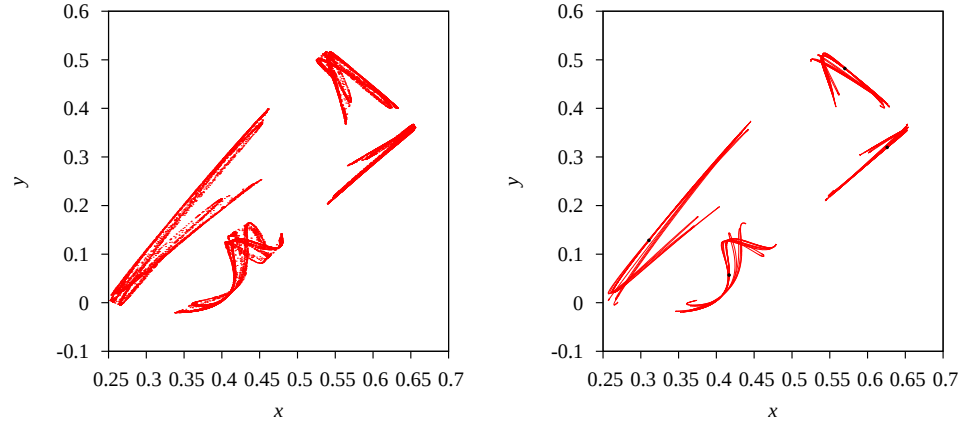

Figure 14: As Figure 13, but for the map $\mathscr{L}$ with $(\alpha, \tau) = (0.28, 2.25)$.

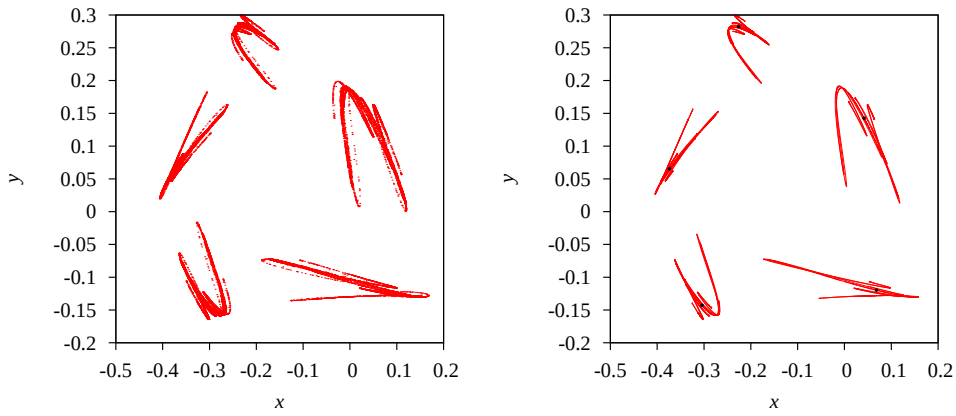

Figure 15: As Figure 13, but for the map $\mathscr{T}$ with $(a, \varphi_d) = (3.43, 148)$.

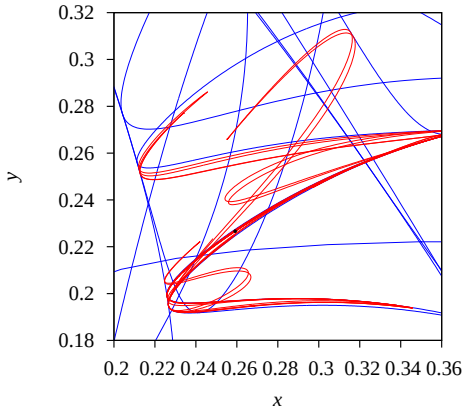

Figure 16: Close up of the Hénon-like attractor of Figure 13 together with some iterates of the critical line LC (in blue).

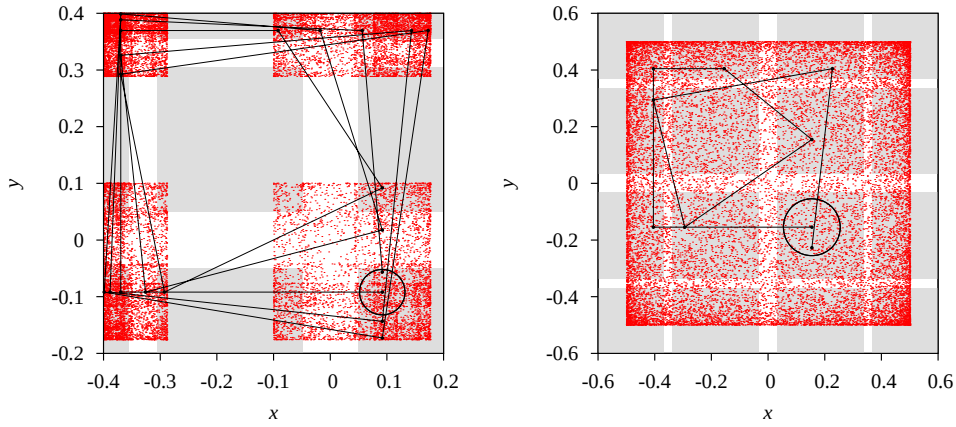

Figure 17: Period-4 points as snapback repellers for $\mathscr{T}^4$ with $\varphi = \pi/2$. The grey areas indicate regions in which the eigenvalues of the matrix $D\mathscr{T}^4$ have an absolute value larger than 1. Line segments between iterates are added for clarity. In the left panel $a = 3.6$ and 20 iterations of $\mathscr{T}$ (i.e., 5 iterations of $\mathscr{T}^4$) are needed to end up in a fixed point of $\mathscr{T}^4$. In the right panel $a = 4$ and only 8 iterations (i.e., 2 iterations of $\mathscr{T}^4$) are needed.

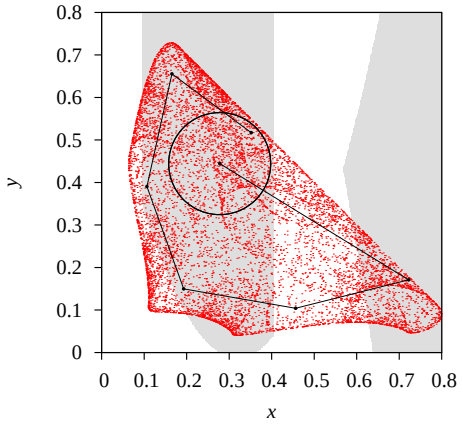

Figure 18: A chaotic attractor of the predator-prey map $\mathscr{P}$ for $(a, b) = (3.6, 3.6)$. The regions for which the Jacobian matrix of $\mathscr{P}$ has two unstable eigenvalues are indicated in grey. The point $(0.277778, 0.444444)$ is an expanding fixed point which is in fact a snapback repeller: an orbit of length 6 of preimages (indicated with dots and line segments to guide the eye) of this point enters a ball of radius $r = 0.12$ around the fixed point.

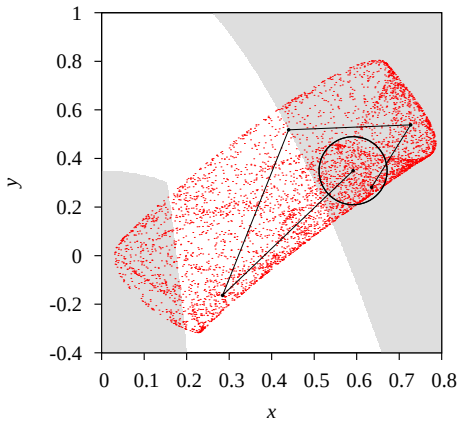

Figure 19: As Figure 19, but for the map $\mathscr{L}$ with $(\alpha, \tau) = (0.35, 2.1)$, the fixed point $(0.591608, 0.35)$, $m = 4$, and $r = 0.08$.

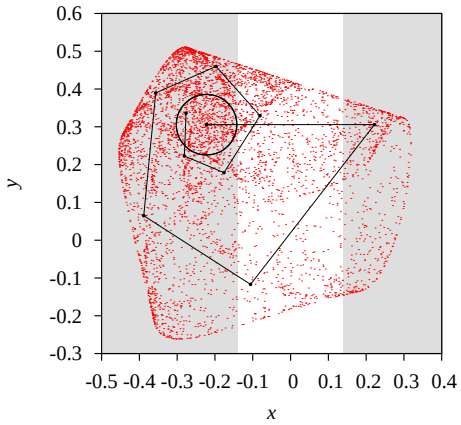

Figure 20: As Figure 19, but for the map $\mathscr{T}$ with $(a, \varphi_d) = (3.6, 72)$, the fixed point $(-0.222222, 0.305863)$, $m = 9$, and $r = 0.08$.

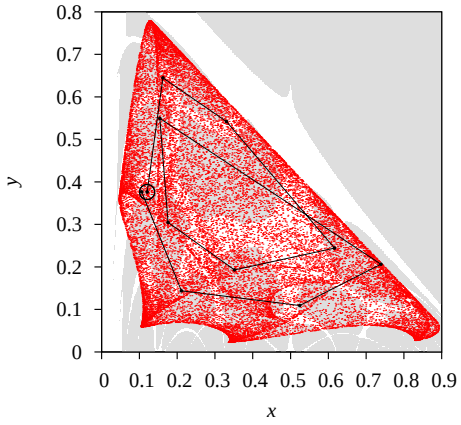

Figure 21: A period-5 point for $\mathscr{P}$ acting as a snap-back repeller for $\mathscr{P}^5$ for $(a, b) = (3.85, 3.6)$. Note that there are 4 more period-5 points which are a snap-back repeller for $\mathscr{P}^5$, but these are not shown.

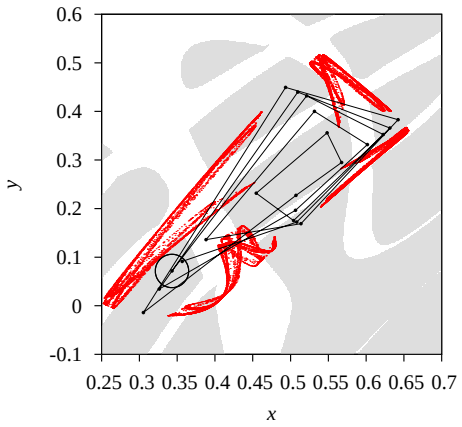

Figure 22: A period-4 point of $\mathscr{L}$ acting as a snap-back repeller for $\mathscr{L}^4$ for $(\alpha, \tau) = (0.28, 2.25)$. Note that there are 3 more period-4 points which are a snap-back repeller for $\mathscr{T}^4$, but these are not shown. These snap-back repellers coexist the Hénon-like attractor for Figure 14.